

Granulysin Crystal Structure and a Structure-derived Lytic Mechanism

Daniel H. Anderson^{1,2*}, Michael R. Sawaya^{1,2}, Duilio Cascio²
William Ernst², Robert Modlin^{2,3}, Alan Krensky⁴ and David Eisenberg^{1,2}

¹Howard Hughes Medical Institute, 5-748 MacDonald Box 951662, Los Angeles, CA 90095-1662, USA

²UCLA-DOE Institute of Genomics and Proteomics Molecular Biology Institute University of California, Los Angeles, Box 951570, Los Angeles, CA 90095-1570, USA

³Division of Dermatology and Dept. of Microbiology, Immunology and Molecular Genetics David Geffen School of Medicine at UCLA, Los Angeles, CA 90095, USA

⁴Department of Paediatrics Stanford University, Stanford CA 94305-5164, USA

Our crystal structure of granulysin suggests a mechanism for lysis of bacterial membranes by granulysin, a 74-residue basic protein from human cytolytic T lymphocyte and natural killer cells. We determined the initial crystal structure of selenomethionyl granulysin by MAD phasing at 2 Å resolution. We present the structure model refined using native diffraction data to 0.96 Å resolution. The five-helical bundle of granulysin resembles other “saposin folds” (such as NK-lysin). Positive charges distribute in a ring around the granulysin molecule, and one face has net positive charge. Sulfate ions bind near the segment of the molecule identified as most membrane-lytic and of highest hydrophobic moment. The ion locations may indicate granulysin’s orientation of initial approach towards the membrane. The crystal packing reveals one way to pack a sheet of granulysin molecules at the cell surface for a concerted lysis effort. The energy of binding granulysin charges to the bacterial membrane could drive the subsequent lytic processes. The loosely packed core facilitates a hinge or scissors motion towards exposure of hydrophobic surface that we propose tunnels the granulysin into the fracturing target membrane.

© 2003 Elsevier Science Ltd. All rights reserved

*Corresponding author

Keywords: granulysin; saposin fold; antimicrobial protein; crystal structure; lytic mechanism

Introduction

Granulysin, a 74-residue basic protein from human cytolytic T lymphocyte and natural killer cells, directly lyses a variety of bacterial, tumor, and fungal cells, including *Mycobacterium tuberculosis* and *Mycobacterium leprae*.¹ Patients expressing large amounts of granulysin can contain the spread of leprosy infection.^{2,3} One visible result of granulysin action on *M. tuberculosis* is the formation of protruding lesions on the target cell surface.¹ Increase in membrane permeability of the *M. tuberculosis* and *Escherichia coli* substrates results in osmotic lysis.⁴ In collaboration with perforin, granulysin kills intracellular *M. tuberculosis* without simultaneous apoptosis.^{5,6} Granulysin can also induce apoptosis of the host cell, in a mechanism involving caspase and other pathways.^{7,8}

Granulysin is one member of the “saposin fold” family of membrane-interacting proteins of various functions. Other examples of the family are: saposins A and C;⁹ porcine NK-lysin;¹⁰ the cyclic peptide bacteriocin AS-48;¹¹ one domain of prophylapsin;¹² and amoebapores.¹³ Saposins A and C appear to alter membranes to become substrates for other enzymes, but do not lyse the membranes they bind. The saposin-like domain of prophylapsin appears to anchor the protein for transport to vacuoles. Bacteriocin protects *Enterococcus faecalis* from bacterial infection by opening pores in the target membrane. NK-lysin and granulysin directly lyse membranes.

Evidence and speculations on the actions of saposin-like proteins have been published. For reviews of antimicrobial peptides and their modes of action, see Zasloff,¹⁴ Shai,¹⁵ and Bechinger.¹⁶ Also, the thinking of Bruhn and Leippe¹³ overlaps that presented here. Qi and Grabowski⁹ propose that differences in charge distributions confer specificity by steering the orientations of saposins

E-mail address of the corresponding author: dha@mbi.ucla.edu

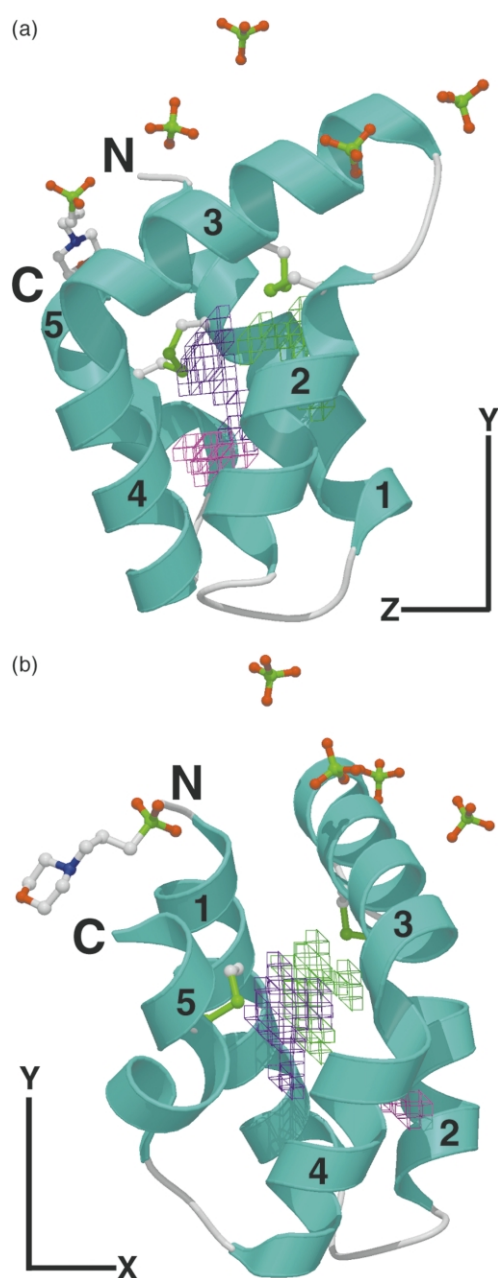


Figure 1. Ribbon representation of the granulysin five-helix bundle. (a) Numbers label helices 1 through 5, and N and C denote N and C termini. Molscript⁵⁴ automatically assigned the backbone geometry as helix (cyan) or coil (white). Molscript interprets the borderline geometry between helices 3 and 4 as a bent helix. The same transition was depicted as coil when the data resolution was 1.5 Å. The two disulfide bonds and the solvent ions (sulfate and N-morpholino propane-sulfonate) are shown as ball-and-stick figures (white carbon, blue nitrogen, red oxygen, green sulfur atoms). Coordination of negative solvent ions in the region at the top of this Figure could indicate the orientation of initial approach to the bacterial membrane. The membrane would run left to right across the top of this Figure (in an x - z plane; see Figure 3). The crystal y direction (indicated at lower right) is slightly tilted from vertical to clarify representation of the voids. (b) Ribbon representation of granulysin seen from the left of (a) (crystal directions are shown at lower left). Disulfide bonds connect helices 1 and 5 (at left) and 2 and 3 (at right).

A and C relative to the membrane surface. The N and C termini were found by them to be buried in the membrane, with a conformational change observed for saposin C. NK-lysin lyses membranes possibly by “molecular electroporation” followed by pore formation.¹⁷ NK-lysin buries its one tryptophan (Trp58) in the membrane but does not lose its secondary structure.¹⁸ Several peptides derived from the NK-lysin and granulysin sequences lyse membranes.^{19,20} Experiments identifying the most lytic peptides do not address the function of the entire molecule, as the protein charge distributions and shape and adjacency effects are not retained in such experiments.

We present our crystal structure of granulysin. Based on interpretation of this structure, and on previous work with membrane-lytic peptides and with other saposin-like proteins, we propose a schematic model of action. The locations of charged solvent species identified in the crystal structure indicate the orientation of granulysin relative to the membrane. The packing of the granulysin in the crystal is a plausible “carpet” arrangement as implicated in the function of other membrane-lytic peptides.¹⁵

Results

Granulysin structure

The granulysin molecule is a five-helix bundle (Figure 1), resembling other “saposin fold” proteins. Our granulysin model includes all 74 residues, of which ten side-chains are split into two conformations each. The granulysin amino acid residues are numbered 1–74, and other modeled species have non-sequential “residue” numbers 81–1107. The model is refined with 0.96 Å resolution diffraction data (R -factor is 0.138; R_{free} for the penultimate model was 0.190). For details and statistics, see Materials and Methods and Table 1.

The granulysin molecules in their crystalline arrangement form many protein–protein contacts in the x and z directions, but few contacts in the y

Hydrophobic side-chains loosely fill the core volume, leaving enclosed voids represented by wire frame. The enclosed volumes identified by VOIDOO (see Materials and Methods) are 14 Å³ (blue), 10.6 Å³ (green), and 5 Å³ (magenta). Unenclosed caves are omitted from this Figure. In the text, we propose that the loose core packing facilitates scissors motion: The left and right helix pairs move out of and into the paper, hinged by backbone torsions in the coil regions at the bottom of this Figure. Preliminary ionic membrane contact drives scissors exposure of hydrophobic surface of the most membrane-lytic portion of the molecule (Helix 3). This Figure was produced with Molscript,⁵⁴ VOIDOO,⁵¹ XtalView,⁵⁵ Raster3D,⁵⁶ and PhotoShop (Adobe).

Table 1. Statistics of the granulysin crystal, data, and model

Resolution shell (Å)	<i>R</i> -factor	$\langle I/\sigma \rangle$	Completeness (%)	
23.6–0.92	0.037	48	82.3	
1.05–1.00	0.129	11	84.6	
1.00–0.96	0.19	6.5	53.4	
0.96–0.92	0.30	3.8	31.7	
Model	<i>R</i> -factor	R_{free}	Peak/hole/ σ	Data/parameters
r13a	0.137 (0.19)	0.190	0.46/ – 0.25/0.052	33821/7094
r13b (1L9L)	0.138 (0.19)	Not evaluated	0.51/ – 0.24/0.058	35633/7094
Restraint	RMS deviation (Å)	Sigma (Å)		
Anti-bump	0.076	0.02		
Bond lengths	0.017	0.02		
Bond distances	0.038 (3°)	0.04		
Flat groups	0.32	0.431		

PDB code: 1L9L. Crystal parameters: space-group $P2_1$, $a = 23.27$ Å, $b = 60.44$ Å, $c = 23.59$ Å, $\beta = 91.0^\circ$. Diffraction data: X-ray wavelength = 0.979 Å. The *R*-factor is calculated on intensities. $\langle I/\sigma \rangle$ is the intensity divided by the error estimate, averaged in a resolution bin. Refinement statistics: The last refinements r13a and r13b were identical except r13b included the R_{free} reflection set. The *R*-factor (calculated on F) is stated for the entire resolution range (23.6–0.92 Å), and in parentheses for the 1.00–0.92 Å shell. Peak/hole refers to the largest positive and negative features in the $F_{\text{obs}} - F_{\text{calc}}$ map (units of electrons Å⁻³), and along with the standard deviation σ indicates the importance of unmodeled structural features. Addition of the former R_{free} reflections further clarified the $F_{\text{obs}} - F_{\text{calc}}$ and $2F_{\text{obs}} - F_{\text{calc}}$ maps, although the σ value increased. A high data-to-parameter ratio encourages stable refinement. Deviations from restraint targets: SHELXL applies its restraints with increasing force as the deviations exceed the sigma values, the expected variabilities in the parameters. The top violators in the anti-bump restraints list are mostly hydrogen atoms. SHELXL restrains bond angles as “bond distances” between one to three atoms. The bond angle deviation in degrees was determined by WHAT_CHECK, and is shown in parentheses. Errors in model parameters were also quantified by full-matrix refinement (see Materials and Methods).

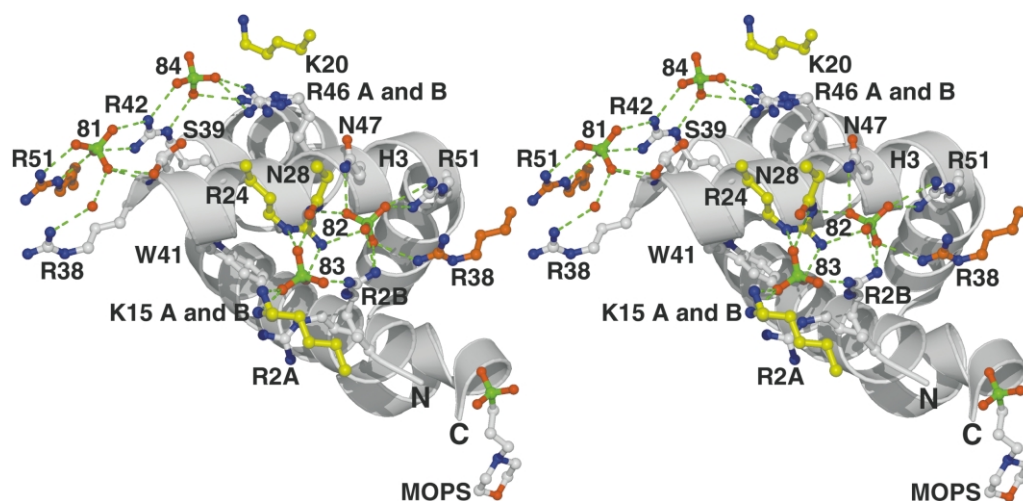


Figure 2. Contacts of sulfate ions. The sulfate hydrogen bonds and salt bridges (combination ionic and hydrogen bond interactions) listed in Table 2 are shown here in a stereo pair. The viewpoint is above Figure 1; crystal axis orientations are the same as in Figure 3. The central granulysin molecule is summarized as light gray ribbons (Helix 3 is labeled H3; termini are labeled N and C). Selected side-chains (identified by one-letter residue codes) and solvent species (for example, 81 means sulfate 81) are shown as ball-and-stick figures. Oxygen atoms are red, nitrogen atoms are blue, and sulfur atoms are green. Carbon atoms of the central molecule are light gray. Symmetry-related granulysin atoms are shown with C atoms colored orange for the same x - z layer, and yellow for the next x - z layer up in the y direction (up refers to Figures 1 and 5). Arg51 at left (R51; orange) is related to Arg51 at right by an $x,y,z - 1$ operation. Arg38 at right (R38; orange) is related to Arg38 at left by an $x,y,z + 1$ operation. The side-chains with yellow atoms are related to the central molecule by a $1 - x,y + 1/2,1 - z$ operation, except Lys15 (K15 at bottom) by $-x,y + 1/2,1 - z$. The location of Trp41 (W41, left of center) indicates the membrane-lytic surface of Helix 3. Both conformations are shown for each discretely disordered side-chain interacting with a sulfate. Sulfate hydrogen bonds and salt bridges are shown as green dotted lines. Some of the electric field interactions are shown by adjacency (see Table 2).

Table 2. Sulfate interactions

Sulfate	Atom	Contacts in model
81	O1	Arg42 NH2
	O2	Arg51 ($x,y,z - 1$) NH2
	O3	Ser39 N and OG_B; water 1011 (indirect to Arg38 NH1)
	O4	Arg42 NH1; Arg51 ($x,y,z - 1$) NE
82	O1	Asn47 ND2; Arg24 ($1 - x,y + 1/2, 1 - z$) NH1
	O2	Arg2_B NH1; Arg38 ($x,y,z + 1$) NH2
	O3	Arg2_B NH1; Arg24 ($1 - x,y + 1/2, 1 - z$) NH2
	O4	Arg51 NH1 and NH2
83	O1	None
	O2	Arg24 ($1 - x,y + 1/2, 1 - z$) NE; Asn28 ($1 - x,y + 1/2, 1 - z$) ND2
	O3	Lys15 ($-x,y + 1/2, 1 - z$) NZ_A and NZ_B
	O4	Arg2_B NH2; Arg24 ($1 - x,y + 1/2, 1 - z$) NH2; unshielded 5–5.5 Å to Arg2_A and Arg40
84	O1	Arg46_A NH1 and NH2
	O2	Arg46_B NH2; Arg42 NE
	O3	Bumps Lys20 ($1 - x,y + 1/2, 1 - z$)
	O4	Arg42 NH1

Hydrogen bond and salt-bridge contacts are shown in Figure 2, and listed here, including non-contact electric field interactions. Alternate conformations are specified by “_A” or “_B” (example: Arg46_A). Symmetry operations specifying adjacent granulysin molecules are stated in fractional coordinates. The sulfate oxygen atoms are located in the N–H directions, except: sulfate 84 bumps the CE atom of the adjacent Lys20, and the Arg2_B N–H–sulfate 82 angle is about 100°.

direction (vertical in Figure 1). Some contacts to ions in the y direction are shown in Figure 2.

Solvent structure

We modeled most of the solvent species as 93 bound water molecules (residue numbers 1001–1107). Three water molecules occupy split sites that follow the conformations and occupancies of their discretely disordered protein anchors (at Gln12, Asp43, Asp72). We also modeled bound molecules of ethanol, N-morpholino propyl-sulfonate (Mops) buffer, and sulfate ions.

We found four sulfate ions bound in an x – z layer (residues 81–84; see top of Figure 1, foregrounds of Figures 2 and 3). The sulfate ions form hydrogen bonds and salt bridges (both ionic and hydrogen bond character) to protein atoms, and presumably respond to electric fields from more distant charged atoms (Figure 2). Table 2 lists the contacts of the sulfate ions. In solution at high ionic strength, distant charges interact weakly.²¹ Below, and in Table 2, we include distant sulfate–protein interactions when in the context of the crystal, no intervening molecules shield their coulombic attractions. Sulfate 81 tightly binds between atoms of granulysin molecules within the same x – z layer. Sulfate 82 tightly binds between atoms within the x – z layer, and Arg24 in the next layer up in the y direction. Sulfate 83 contacts Arg2 in its conformation B but otherwise experiences electric field from the other conformation of Arg2, Arg40, and atoms of the next molecule up in the y -direction. Residual density at sulfate 83 could represent an overlapping binding site nearer Arg2 conformation A, and Arg40. Sulfate 84 is the least tightly held in this model, judging from its electron density. Sulfate 84 contacts atoms in one granulysin molecule, and bumps (no salt bridge) Lys20 of an adjacent molecule

in the next x – z layer up along the y direction. In Discussion, below, we will infer mechanism partly from the observation of crystal packing in alternating sheets of protein and solvent ions.

A molecule of Mops buffer binds between the N and C termini (top of Figure 1). The morpholine ring is in chair conformation. The ring nitrogen is protonated and forms a salt bridge to the C-terminal Arg74 carboxylate. The ring oxygen directs its electron clouds towards an Arg42 in the same x – z layer. The sulfonate and the first carbon of the propyl group appear (because of the poorly-shaped streak of density) to adopt an overlapping series of positions near the N-terminal Gly1 amine and the side-chain of Arg50 of an adjacent granulysin molecule in the same x – z layer. The Mops sulfonate thus appears to interact with the local electric field, rather than in direct salt bridges as do the more tightly held sulfate ions.

During model building and refinement, our model left residual electron density in the solvent region. The most prominent un-modeled features in the solvent were of about the diameter of a sulfate ion, sliding over the modeled and un-modeled commotion of positive charges brought together by crystal symmetry: arginine residues 2, 5, 32, 35, 46, and Lys20. With current crystallographic methods, we can model atoms only in discrete, highly populated states.

Voids in the hydrophobic core

By visual inspection of the granulysin model, we found enclosed cavities lined by hydrophobic atoms in the loosely packed core. To quantify core looseness, rather than to identify ligand-binding sites, we used the VOIDOO program (see Materials and Methods) with probe radius of 0.5 Å. By this method, we found that the three largest voids

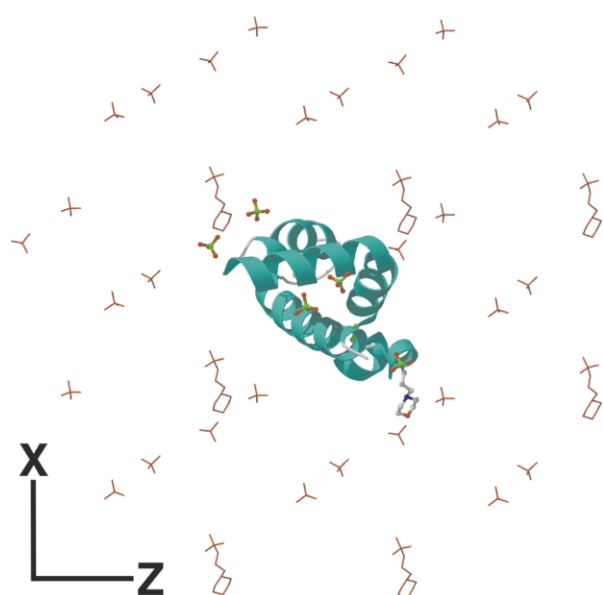


Figure 3. Charged solvent species layer in the granulysin crystal. The crystal contains x - z sheets of granulysin molecules, interleaved with x - z sheets of sulfate and Mops molecules. The viewpoint is from the top of Figure 1, same orientation (shown lower left) but more distant than in Figure 2. The granulysin molecule is shown at center, in ribbon representation. The four sulfate ions straddle Helix 3, and contact neighboring granulysin molecules as described in the text and Table 2, and illustrated in Figure 2. The Mops buffer bridges the N and C termini. The repeating red stick figures represent symmetry-related sulfate and Mops molecules, bound in a nearly flat x - z layer. The granulysin similarly repeats by translation in the crystal. In the text we propose that the layer of charged species in the crystal could represent the negative charges of the bacterial membrane. The viewpoint in this Figure would then be inside the bacterial cell, looking “out the window” at the first-arrived granulysin molecule, with its most membrane-lytic Helix 3 pressed against membrane surface charges.

enclose 14 \AA^3 , 11 \AA^3 , and 5 \AA^3 (total volume 30 \AA^3 ; see Figure 1). The same analysis applied to the plant-specific (saposin) domain of the prophytpsin crystal structure (PDB accession code 1QDM)¹² detected voids surrounding Met79S (about 15 \AA^3 in chain A, 14 \AA^3 in chain B, 10 \AA^3 in chain C). The NMR models of NK-lysin (1NKL),¹⁰ and bacteriocin (1E68)¹¹ are more loosely packed than the crystal structures, and VOIDOO detected many voids, tunnels and caves. For NK-lysin, the enclosed voids were more than double the volumes found in granulysin. In Discussion, below, we propose that the loose core packing participates in the membrane-lytic activity of granulysin.

Hydrophobic moments

The granulysin molecule is a small, hydrophobic-core, helical bundle, only two helices thick,

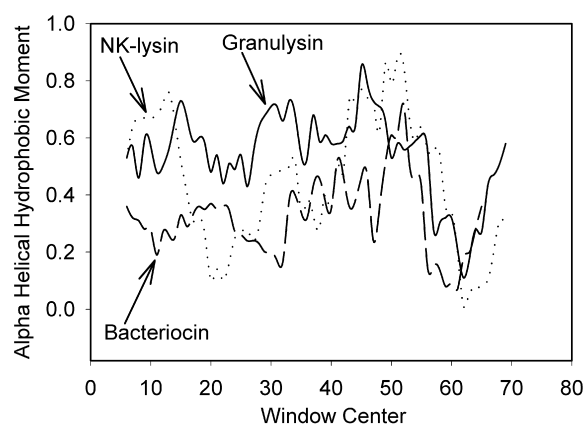


Figure 4. Hydrophobic moments of three “saposin fold” sequences. Moderately large values of calculated hydrophobic moments suggest the presence of membrane-lytic segments.²² Hydrophobic moments were calculated assuming that each polypeptide chain is entirely α -helical, and using the default 11-residue window (thus, the first function value is centered at residue 6). We rearranged the sequence file of the cyclic polypeptide bacteriocin AS-48¹¹ (N and C termini fused in “Helix 5”; sequence modified to 10–70, 1–9). The maximum hydrophobic moments in granulysin and NK-lysin are in α -helices previously identified as membrane-lytic.^{19,20}

and is almost entirely amphipathic. The “hydrophobic moment” function quantifies how amphipathic a sequence segment is, assuming helicity (see Materials and Methods). Moderately large calculated hydrophobic moments are correlated with membrane-lytic segments of amino acid sequences.²² We calculated the hydrophobic moments of granulysin and related sequences, and show results for three sequences in Figure 4. The peak values of hydrophobic moment range from large in the strongly membrane-lytic proteins granulysin and NK-lysin, to above background in the simply membrane-interacting proteins (saposin domain of prophytpsin; saposins A, B, C, D). The residues at moment maxima reside mostly in helices, several at ends of helices. The value of the hydrophobic moment function may be reduced by hydrophobic domain interfaces or exposed hydrophobic surface, as in bacteriocin.¹¹ For granulysin and NK-lysin, the hydrophobic moment function reaches maxima in segments that in tests of synthetic peptides had been previously identified as membrane-lytic.^{19,20}

Discussion

From the structural detail observed *via* crystallography, we extrapolate to the function of granulysin on the target cell membrane, assisted by the sparse matrix of previous experiments and thoughts on related membrane-lytic proteins. The granulysin structure implies its function, but not

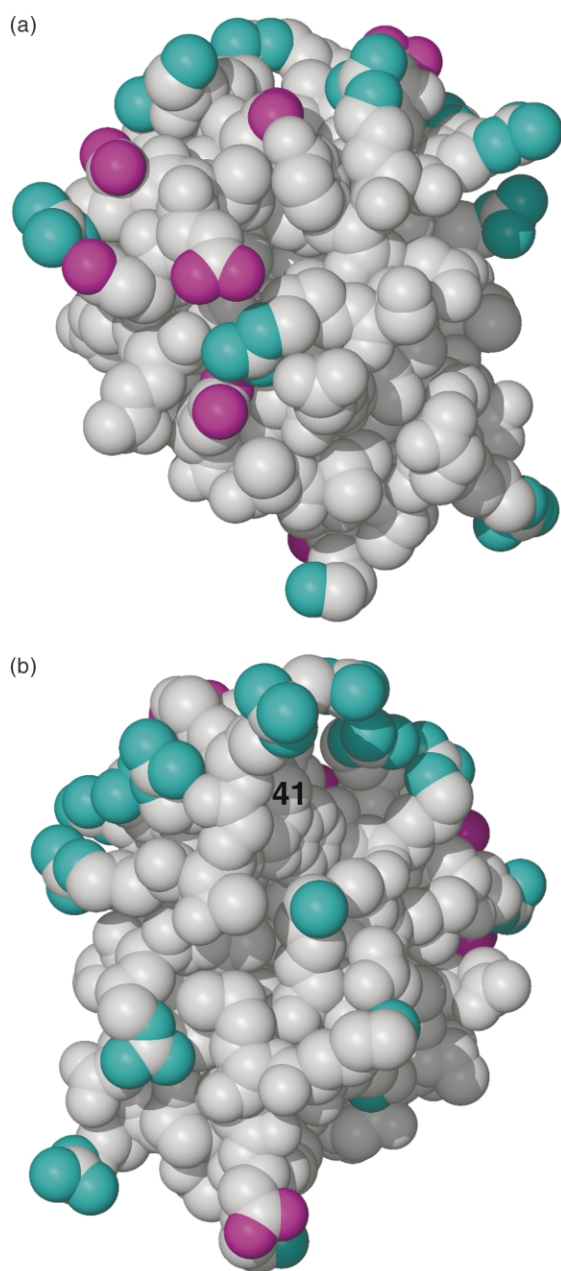


Figure 5. Granulysin charge locations. The charge distribution in the granulysin molecule steers its orientation relative to the membrane. All the protein atoms are shown as balls (but excluding all conformation B atoms). Positively charged atoms (N-terminal amine, Lys and Arg side-chain nitrogen atoms) are cyan. Negatively charged atoms (oxygen atoms of Asp and Glu side-chains, and the C-terminal carboxylate) are magenta. (a) View as in Figure 1(b). Positive charges distribute mostly in a ring around the molecule, with greatest concentration at the top. Most of this face is uncharged polar. Tyrosine 52 and Leu73 are partly exposed near the top of this region. (b) View from behind Figure 1(b), right side of Figure 1(a), left side of Figure 2. Many backbone atoms are exposed on this face. Trp41 is in a cleft near the top (atom CB marked 41). Val33 and Met17 are exposed near the middle. In the context of the crystal, several long charged groups turn their charged atoms away, exposing their methylene chains on this face. The positive charge concentration of granulysin steers the sulfate ions into a layer in the crystal (top of

as explicitly as would a ligand-bound enzyme structure. We narrow discussion to lysis of bacterial membranes in culture. On an exposed substrate, the action of granulysin is not complicated by partners in translocation, such as perforin and caspase (see Introduction). The outermost layers of bacterial cells (lipopolysaccharides, peptidoglycan, teichoic acids) appear to be too porous to exclude granulysin by dialysis. Traversing a tightly woven structure would require application of an injecting force, and could cause some conformation changes preceding those we discuss, below.

Initial contacts

The initial contact between a granulysin molecule and a bacterial membrane is likely mediated by arginine charges attracted to the layer of membrane phosphate charges. Granulysin membrane binding and lysis may be inactivated by chemical modification of its arginine residues.⁴ In the granulysin crystal, the negative solvent ions (four sulfate sites per granulysin monomer) bind between arginine charges in an $x-z$ layer (top of Figure 1; foregrounds of Figures 2 and 3). The Mops buffer places its sulfonate near the N terminus. The ion binding geometry in the crystal results in part from the allowed side-chain conformations in that restrictive environment. As in many other crystal structures, some side-chains of granulysin adopt two conformations (examples in Figure 2). On a bacterial membrane, the charged side-chains of granulysin would search for contacts by sampling conformations. The granulysin charge cluster coordinating negative charges as seen in the crystal (cyan atoms at top of Figure 5), will do so in the solution environment.

The negative ions in the crystal bind near Helix 3, the most membrane-lytic portion of the granulysin molecule, as identified by testing for lysis by synthetic peptides derived from granulysin and NK-lysin.^{4,19,20} Also, the hydrophobic moment function reaches its maximum in Helix 3 (see Results and Figure 4).

The accumulated observations and parallels indicate that the initial contacts of the granulysin molecule to the target membrane are at the tops of Figures 1 and 5, and in the foregrounds of Figures 2 and 3. Saposins A and C bury their N and C termini in the target membrane.⁹ Miteva *et al.*¹⁷ calculated potentials around the NK-lysin NMR model, and proposed the same initial contacts. Their Figure 1(c) (NK-lysin on hypothetical membrane) differs in style and in viewpoint from our Figure 3 (granulysin on sulfates plane in the same relative orientation).

Figure 1, foregrounds of Figures 2 and 3), and could orient the granulysin molecule relative to a negatively charged membrane. After rolling, this face could be the second to interact with the membrane. This Figure was produced with XtalView⁵⁵ and Raster3D.⁵⁶

Bruhn and Leippe¹³ did not predict the orientation of their amoebapore model relative to the membrane for lack of charge clusters.

Positive charges not involved in initial contact with the membrane would sustain force to drive granulysin into the membrane surface, and could drive subsequent events. The surface of granulysin facing the viewer in Figure 5(b) is a plausible candidate for secondary interactions (the face in Figure 5(a) is too hydrophilic). Val33, Trp41 and Met17 are among the hydrophobic groups located on this face. Positive charges on this face could roll the granulysin molecule around the N termini of helices 1 and 3, bringing the lytic surfaces of helices 1, 2, and 3 nearer the target membrane.

Granulysin has one tryptophan (Trp41), located at the N terminus of Helix 3, in the most lytic segment of the sequence. In the granulysin crystal structure, Trp41 nests in a cleft (left of center in Figure 2; near the top of Figure 5(b)), but may be rotated out (χ_1 rotation) without serious collisions, even without postulating further structural rearrangement induced by contact with a membrane. Once the granulysin molecule orients *via* charges at the membrane surface, Trp41 could easily insert into the membrane as disruption of the membrane initiates. Tryptophan residues have been implicated in the anchoring function of phospholipases A₂, and we have inferred a similar function in *M. tuberculosis* antigen 85B.²³ NK-lysin partially buries its only tryptophan in the membrane¹⁸ (Trp58, exposed to solvent in Helix 4). In Figure 1(c) of Miteva *et al.*,¹⁷ based on energy calculations, the Trp58 of NK-lysin faces away from the proposed location of the membrane. NK-lysin may approach the membrane at a different angle, or penetrate deeply.

Voids facilitate scissoring

The voids in the hydrophobic core of granulysin may allow relative motion of the helical halves of the molecule on binding to the bacterial membrane. The cavities are not large enough for insertion of a ligand such as a phospholipid molecule, unless the granulysin molecule opens (see below, and Results). Disulfide bonds hold together granulysin Helix 1 with Helix 5, and Helix 2 with Helix 3 (left and right sides of the ribbon representation in Figure 1(b)). NK-lysin is inactivated by reduction of its disulfide bonds²⁴ as though the halves need tethering. The covalent backbone link from Trp70 to Met1 in the cyclic polypeptide bacteriocin appears to provide sufficient rigidity without disulfides. Without fully interdigitated side-chains, the oily (rather than waxy) core of granulysin would allow a scissors motion of the disulfide-linked helix pairs (1–5 and 2–3; out of and into the paper, Figure 1(b)), exposing the lytic inner surfaces to the bacterial membrane. We think that a scissors motion would precede any gross turning inside-out because it would require less energy, and only some backbone torsions in the region of residues 17–20 and near Ala62. We found

evidence of backbone twist at Leu60 (see Materials and Methods). Some peptides derived from the granulysin sequence can lyse membranes, above threshold concentrations. These segments are pre-clustered in intact granulysin, and the full structure lyses with no threshold detected.⁴ The energy of charge binding and subsequent rolling could drive a scissors motion exposing more membrane-lytic surface. This charge-driven scissors motion could be the process underlying “molecular electroporation”.¹⁷

The cavity volumes we report are not directly comparable to those reported elsewhere (for example in Ref. 25). Internal voids have been found in many proteins, including NK-lysin,¹⁰ in predicted structures of amoebapores,¹³ and many crystal structure reports mention internal cavities. Voids in the structure of colicin E1, for example, were proposed to facilitate structural rearrangement during the action of that molecule.²⁶ Peristaltic rearrangement of internal cavities appears to move ligand molecules through “solid” myoglobin.²⁷ In their analysis of domain:domain motions facilitated by internal cavities, Hubbard and Argos²⁸ used larger probe spheres than we did. That our 1 Å diameter probe sphere can roll between some granulysin core atoms drawn at their van der Waals radii indicates that these atoms can pass each other with little friction.

Cooperative membrane fracturing

Many granulysin molecules may participate in each membrane lesion (see Figure 4 of Stenger *et al.*¹). The lesions are much larger than individual granulysin molecules. Granulysin can kill a bacterial cell within minutes by increase of membrane permeability.⁴ The several-days time scale of lesioning by granulysin could mean that formation of lesions proceeds stepwise as more granulysin molecules aggregate at the bacterial membrane. Addition of ammonium sulfate to a granulysin solution crystallized the granulysin into tightly packed *x*–*z* protein layers alternating with sulfate/Mops layers. If granulysin aggregates at the charged layer on a membrane surface, one plausible way the granulysin molecules can interact is *via* the interfaces displayed in the densely packed crystalline *x*–*z* plane. The crystalline arrangement in the *y* direction is mediated by sulfate ions and very few protein–protein contacts (vertical in Figures 1 and 5; perpendicular to the paper in Figures 2 and 3). Shai¹⁵ suggests an initial “carpeting” of the membrane by lytic peptides. Yang *et al.*²⁹ report crystalline arrangements of membrane pores formed by magainins and protegrins, above the critical peptide to lipid ratios. Magainin and melittin may be cyclized (*via* cysteine residues added at N and C termini; presumably while unfolded), and retain some lytic activity.³⁰ This suggests that carpeting the membrane is enough for lysis; insertion of linear helices (prevented by disulfide cyclization) is not mandatory. A geometric clustering of granulysin could accommodate a non-geometric distribution

of membrane charges by searching side-chain conformations. A preference for semi-periodic charge arrays could provide some target membrane specificity.

A dense clustering of granulysin molecules could allow cooperative lysis by "friction" between adjacent molecules. In the example "carpet" of the crystalline packing, Asp3 and Lys13 salt bridge to Arg38 and Asp72 of the next granulysin molecules in the $\pm z$ directions. These ion pairs, and other interactions, would help hold together a row of granulysin molecules in the z direction. A rotation of the row of molecules around an axis parallel with z , while maintaining a dense carpet, would stress and deform the granulysin (*via* collisions) and the membrane. Each granulysin molecule could apply local forces to its patch of membrane, and its structure rearrange through a series of conformations as newly neighboring granulysin molecules locally bend their membrane patches. Matsuzaki³¹ discusses cumulative curvature stress by magainin and tachyplesin peptides. The granulysin-induced lesions may represent accumulation of many local bending events.

Conclusion

Based on our crystal structure of granulysin and on published work with this and other antimicrobial proteins, we have presented a model that seems plausible for events leading to membrane lysis. These are summarized in the low-resolution cartoons of Figure 6. We do not have direct evidence of periodic aggregation of granulysin on the membrane, as reported for magainin and protegrin by Yang *et al.*²⁹ To induce crystallization, we counteract the entropy of granulysin in solution by addition of a high concentration of ammonium sulfate. On a bacterial surface, the negative charges are already confined in a layer, and thus granulysin can spontaneously aggregate on it as a dense carpet. Minton³² explains the thermodynamics of surface adsorption and two-dimensional crystallization *via* weak self-association. The apparent lack of threshold concentration⁴ indicates that granulysin molecules start lysis singly or in small rugs. Our extrapolation from the crystalline x - z plane of negative solvent charges to the surface of a bacterial cell seems plausible.

Materials and Methods

Crystallization

Granulysin was produced and purified as described,^{4,33} but scaled up to 5 mg injections into a larger reverse-phase column (Varian Dynamax C18; 21.4 mm \times 25 cm, plus guard cartridge). The flow rate was 10 ml min⁻¹, and detection was by absorbance at 280 nm. The granulysin peak fractions were dried in a vacuum centrifuge (Speed Vac from Savant) for storage. The dried granulysin was dissolved to about 10 mg ml⁻¹ by addition of water. Crystals grew by the hanging drop

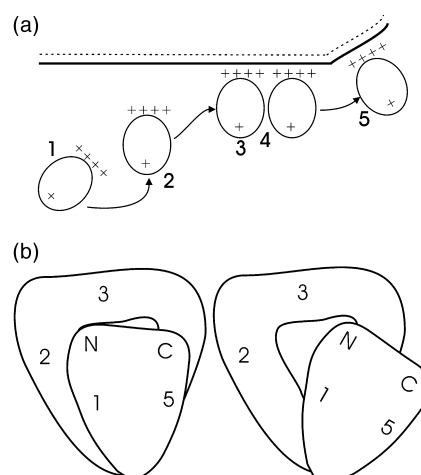


Figure 6. Schematic diagrams of granulysin action. (a) Ellipses represent granulysin molecules, with a cluster of positive charges (++++), and more positive charges distributed elsewhere (+; see Figure 5). The charge cluster of the granulysin molecule in solution (1) orients the molecule (2) towards the negatively charged surface of the bacterial cell (line with dashes). The arginine residues bind surface charges (3). The granulysin molecules could cluster at the cell surface (4), possibly as in the crystal: x - z sheets of granulysin alternating with x - z sheets of sulfate ions and Mops. This arrangement clusters the N and C termini and the most lytic helix adjacent to the sulfate (membrane) layer. Granulysin lyses the membrane (5), possibly rolling the granulysin in the direction of the lytic surfaces of helices 1, 2, and 3 (see Figure 5(b)). (b) The lysis process could involve a scissors motion enabled by the internal voids (see Figure 1), further exposing lytic surface. Granulysin's terminal helices 1 and 5 (gray foreground object) are disulfide-linked, and would move together. Helices 2 and 3 are also disulfide-linked. The most membrane-lytic surfaces are in helices 1, 2 and 3 (see Figure 4). The helical sheets could slide past each other, lubricated by the loose and thus oily core, hinged at the bottoms of this diagram and of Figure 1. Such a conformation change, driven by rolling and bringing more charges nearer the membrane, could expose more lytic surface, and dig the granulysin into the membrane, bending or tearing it.

vapor diffusion method. The reservoir solutions were 1 ml of 3.1–3.2 M (NH₄)₂SO₄, 0.05 M Na Mops (pH 7), 2.5% (v/v) ethanol. The drops contained equal volumes of 10 mg ml⁻¹ granulysin in water, and reservoir solution from the 3.2 M condition. This granulysin/precipitant mixture was centrifuged at 9700g for 5 min, and 4 μ l drops were pipetted onto siliconized cover slips. The granulysin crystals began growing about two weeks later at 21–22 °C. The growth processes continued for at least a month. Most granulysin crystals grew as clusters. Presence of ethanol reduced the number of crystals per cluster, and sometimes yielded the single crystals that we used for this work. A different crystal morphology resulted from substitution of ethanol by acetone or 2-methyl-2,4-pentanediol (MPD). The MPD form crystals were much softer and diffracted more poorly than the ethanol form. The MPD and ethanol form crystals appear to be nearly isomorphous, and MPD binds weakly or not

at all. All crystals used here were flash-frozen in “cryosalt”,³⁴ consisting of 0.8 volume of saturated $(\text{NH}_4)_2\text{SO}_4$ and 0.2 volume of saturated lithium acetate.

The granulysin crystal symmetry is $P2_1$, with cell dimensions $a = 23.27 \text{ \AA}$, $b = 60.44 \text{ \AA}$, $c = 23.59 \text{ \AA}$, and $\beta = 91.0^\circ$. Because the a and c cell parameters are almost equal, many data sets had to be re-indexed (h, k, l became $l, -k, h$). However, we found no evidence of merohedral twinning that could have resulted from this lattice geometry.³⁵

Structure determination

Selenomethionyl granulysin was prepared in *E. coli* by means of providing selenomethionine while stopping methionine biosynthesis.³⁶ One useable crystal grew and was frozen as above. Diffraction data were collected at Brookhaven National Laboratory Beamline X8C at wavelengths corresponding to the peak, inflection, and a high-energy remote.³⁷ The detector was an Area Detectors Systems Corporation Quantum 4R. Diffraction data were processed with HKL.³⁸ Anomalous and dispersive difference Patterson functions showed 10 σ peaks representing the two Se atoms. Se coordinates were found with SHELXD.³⁹ Selenium parameters were refined and phases calculated up to 2 \AA resolution with MLP-HARE.^{40,41} These rough phases were modified by solvent flattening and histogram matching in resolution shells, and extended to 1.5 \AA , using DM.^{41,42} The modified phases were input for refinement and automatic model building using ARP/wARP.⁴³ Almost the entire granulysin molecule (but not Gly1 or Lys13), and much of the solvent structure were thus automatically placed using the selenomethionine diffraction data.

Refinement

The ARP/wARP protein model (no solvent) was then refined with native (sulfur methionine) diffraction data, using SHELXL⁴⁴ in conjugate gradient mode. For the first five rounds of refinement, we used a 1.5 \AA resolution in-house data set, collected with Cu $K\alpha$ radiation and an ADSC Quantum 4 CCD detector. For refinements 6 through 13, we used diffraction intensities measured at Beamline X8C, as before. High-resolution data were collected at 30 seconds exposure time, with crystal-to-detector distance of 60 mm. The more intense low-resolution data were collected at five seconds exposure time, at a distance of 120 mm. The wavelength was 0.979 \AA . Statistics of the high-resolution data set are listed in Table 1. The same reflections were tagged for R_{free} calculation throughout the refinement process. Surprisingly, several side-chains flipped during the change between data sets. The amino acid sequence of the granulysin model was altered in response to the electron density: The structure we report has isoleucine in position 57 (PIR data base sequence code A27562), not the Thr57 variant as was input to ARP/wARP.

We restrained the geometries of granulysin and its small-molecule ligands. Sulfate and ethanol coordinates were obtained from the Cambridge Crystal Structure Database,⁴⁵ and were used as restraint targets for SHELXL refinement. Coordinates of Mops were obtained from the HIC-up database of protein ligand structures.⁴⁶ Refinement with granulysin data symmetrized the input morpholine ring structure, and that symmetry was later enforced by symmetric restraint values. Globally decreasing the rigidities of the geometric restraints did

not alter R_{free} , and we therefore used the default restraint stringencies.

Content of the granulysin model

The granulysin model includes hydrogen atoms, primarily to apply the hydrogen anti-bump restraint in SHELXL. Few of the hydrogen atoms are sufficiently localized to produce easily visible electron density. All non-hydrogen atoms of the model are anisotropic. We also used the overall anisotropic scaling and bulk solvent scaling features of SHELXL. Occupancy parameters for split side-chains and their associated water molecules were refined by SHELXL. We manually input unrefined occupancy parameters of 0.5 for some water molecules, and for sulfate ions 83 and 84, to qualitatively scale the electrons of the model to the strength of the electron density calculated from the diffraction data. At each water site, the U^{ij} parameters mimic the distribution about the average. Three water molecules occupy split sites that follow the conformations and occupancies of their protein anchors (at Gln12, Asp43, Asp72). Not all atoms of the model may be present simultaneously. The side-chains of Gln12 and Asp72 of adjacent molecules in the same $x-z$ layer may simultaneously occupy their A conformations, while binding water molecules 1021A and 1041A. Either side-chain in conformation B excludes water 1021B.

We added detail to the model until the standard deviation (σ) and features of the $F_{\text{obs}} - F_{\text{calc}}$ map (Table 1) decreased to insignificance. The protein model excludes some interpretable details, for example: difference peaks indicate that a few percent of the disulfide bridges between Cys35 and Cys45 are broken, possibly due to radiation damage. The side-chain of Leu60 has a very low occupancy second conformation, whose modeling would require a backbone twist, and thus a disproportionate complication of the model.

Validation of the model

We judge the granulysin model to be of good quality. Statistics of the refinement and the model are presented in Table 1. The model fits the density, by visual examination. The outputs of SHELXL, PROCHECK⁴⁷ and WHAT_CHECK⁴⁸ did not indicate significant problems, except as noted in the next paragraph. All residues are in favorable backbone conformations according to a Ramachandran ϕ - ψ plot⁴⁹ except that Asp19 is in an “additionally allowed” region. Aspartate 19 is bent by its location at the end of Helix 1, and stretched by adjacent arginine charges; Asp19 thus does not relax into a Ramachandran favored conformation.

Errors in the granulysin model were further quantified by full-matrix refinement using SHELXL with enlarged arrays. This method estimates uncertainties in model parameters without reference to geometric restraint targets. The starting model for this calculation was the all-data model r13b (1L9L; Table 1). For most atoms, the estimated positional errors cluster tightly around 0.02–0.05 \AA . Estimated errors in principal U^{ij} values are mostly 5–10%. The worst parts of the granulysin model are Arg2 and Arg35. The two modeled conformations of Arg2 only partially explain the events at this site. In placing atoms of Arg2, conformation A, at their average positions, the refinement gradients visibly bent the CD–NE–CZ bond angle 18° away from its target value. Still, the estimated errors in the average positions of these atoms are only 0.05–0.07 \AA . In contrast, the terminal atoms of Arg35 are

very near target geometry, but the estimated positional errors reach as high as 0.17 Å for atom NH1 in conformation A.

Computations

Hydrophobic moments were computed with the MOMENT program[†]. We used the default 11-residue window, and assumed helicity of all segments. Hollows were evaluated with the “molecular speleology” program VOIDOO.⁵⁰ We removed the hydrogen atoms from the models for consistent evaluation of voids. To quantify the volumes between core side-chains, rather than volumes available to a ligand, we reduced the probe radius from its default value of 1.4 Å to 0.5 Å. When unavailable, three-dimensional models were constructed for saposin-like sequences by threading onto the granulysin crystal structure using SWISS-MODEL.^{51,52}

Atomic coordinates

The granulysin diffraction data and the model reported here (r13b in Table 1) have been deposited in the RCSB Protein Data Bank[‡] under accession code 1L9L.

Acknowledgements

We thank Peter Müller for assistance with handling of diffraction data, and Annaliza Legaspi for production of granulysin. This work was supported by: NIH grants AI07118 and AR40312 to R.M. and AI43348 to A.K.; HHMI award to D.E. This material is based upon work supported by the National Science Foundation under grant number 9904671 to D.E.

References

- Stenger, S., Hanson, D. A., Teitelbaum, R., Dewan, P., Niazi, K. R., Froelich, C. J. *et al.* (1998). An antimicrobial activity of cytolytic T cells mediated by granulysin. *Science*, **282**, 121–125.
- Stenger, S. (2001). Cytolytic T cells in the immune response to *Mycobacterium tuberculosis*. *Scand. J. Infect. Dis.* **33**, 483–487.
- Ochoa, M.-T., Stenger, S., Sieling, P. A., Thoma-Uszynski, S., Sabet, S., Cho, S. *et al.* (2001). T cell release of granulysin contributes to host defense in leprosy. *Nature Med.* **7**, 174–179.
- Ernst, W., Thoma-Uszynski, S., Teitelbaum, R., Ko, C., Hanson, D. A., Clayberger, C. *et al.* (2000). Granulysin, a T cell product, kills bacteria by altering membrane permeability. *J. Immunol.* **165**, 7102–7108.
- Dieli, F., Troye-Blomberg, M., Ivanyi, J., Fournié, J. J., Krensky, A., Bonneville, M. *et al.* (2001). Granulysin-dependent killing of intracellular and extracellular *Mycobacterium tuberculosis* by Vgamma9/Vdelta2 T lymphocytes. *J. Infect. Dis.* **184**, 1082–1085.
- Thoma-Uszynski, S., Stenger, S. & Modlin, R. (2000). CTL-mediated killing of intracellular *Mycobacterium tuberculosis* is independent of target cell nuclear apoptosis. *J. Immunol.* **165**, 5773–5779.
- Kaspar, A., Okada, S., Kumar, J., Poulain, F. R., Drouvalakis, K. A., Kelekar, A. *et al.* (2001). A distinct pathway of cell-mediated apoptosis initiated by granulysin. *J. Immunol.* **167**, 350–356.
- Pardo, J., Pérez-Galán, P., Gamen, S., Marzo, I., Monleón, I., Kaspar, A. *et al.* (2001). A role of the mitochondrial apoptosis-inducing factor in granulysin-induced apoptosis. *J. Immunol.* **167**, 1222–1229.
- Qi, X. & Grabowski, G. A. (2001). Differential membrane interactions of saposins A and C: implications for the functional specificity. *J. Biol. Chem.* **276**, 27010–27017.
- Liepinsh, E., Andersson, M., Ruyschaert, J.-M. & Otting, G. (1997). Saposin fold revealed by the NMR structure of NK-lysin. *Nature Struct. Biol.* **4**, 793–795.
- González, C., Langdon, G. M., Bruix, M., Gálvez, A., Valdivia, E., Maqueda, M. & Rico, M. (2000). Bacteriocin AS-48, a microbial cyclic polypeptide structurally and functionally related to mammalian NK-lysin. *Proc. Natl Acad. Sci. USA*, **97**, 11221–11226.
- Kervinen, J., Tobin, G. J., Costa, J., Waugh, D. S., Wlodawer, A. & Zdanov, A. (1999). Crystal structure of plant aspartic proteinase prophytepsin: inactivation and vacuolar targeting. *EMBO J.* **18**, 3947–3955.
- Bruhn, H. & Leippe, M. (1999). Comparative modeling of amoebapores and granulysin based on the NK-lysin structure: structural and functional implications. *Biol. Chem.* **380**, 1001–1007.
- Zaslhoff, M. (2002). Antimicrobial peptides of multicellular organisms. *Nature*, **215**, 389–395.
- Shai, Y. (1999). Mechanism of the binding, insertion and destabilization of phospholipid bilayer membranes by alpha-helical antimicrobial and cell non-selective membrane-lytic peptides. *Biochim. Biophys. Acta*, **1462**, 55–70.
- Bechinger, B. (1997). Structure and functions of channel-forming peptides: magainins, cecropins, melittin and alamethicin. *J. Membr. Biol.* **9156**, 197–211.
- Miteva, M., Andersson, M., Karshikoff, A. & Otting, G. (1999). Molecular electroporation: a unifying concept for the description of membrane pore formation by antibacterial peptides, exemplified with NK-lysin. *FEBS Letters*, **462**, 155–158.
- Ruyschaert, J.-M., Goormaghtigh, E., Homblé, F., Andersson, M., Liepinsh, E. & Otting, G. (1998). Lipid membrane binding of NK-lysin. *FEBS Letters*, **425**, 341–344.
- Wang, Z., Choice, E., Kaspar, A., Hanson, D. A., Okada, S., Lyu, S.-C. *et al.* (2000). Bactericidal and tumoricidal activities of synthetic peptides derived from granulysin. *J. Immunol.* **165**, 1486–1490.
- Andreu, D., Carreño, C., Linde, C., Boman, H. G. & Andersson, M. (1999). Identification of an anti-mycobacterial domain in NK-lysin and granulysin. *Biochem. J.* **344**, 845–849.
- Lee, K. K., Fitch, C. A. & García-Moreno, B. E. (2002). Distance dependence and salt sensitivity of pairwise, coulombic interactions in a protein. *Protein Sci.* **11**, 1004–1016.
- Eisenberg, D. & Wesson, M. (1990). The most highly amphiphilic alpha-helices include two amino acid segments in human immunodeficiency virus glycoprotein 41. *Biopolymers*, **29**, 171–177.
- Anderson, D. H., Harth, G., Horwitz, M. A. & Eisenberg, D. (2001). An interfacial mechanism and

[†] <http://www.doe-mbi.ucla.edu/Services/moment>

[‡] <http://www.rcsb.org/pdb/>

- a class of inhibitors inferred from two crystal structures of the *Mycobacterium tuberculosis* 30 kDa major secretory protein (antigen 85B), a mycolyl transferase. *J. Mol. Biol.* **307**, 671–681.
24. Andersson, M., Holmgren, A. & Spyrou, G. (1996). NK-lysin, a disulfide-containing effector peptide of T-lymphocytes, is reduced and inactivated by human thioredoxin reductase: implication for a protective mechanism against NK-lysin cytotoxicity. *J. Biol. Chem.* **271**, 10116–10120.
 25. Hubbard, S. J., Gross, K.-H. & Argos, P. (1994). Intramolecular cavities in globular proteins. *Protein Eng.* **7**, 613–626.
 26. Elkins, P., Bunker, A., Cramer, W. A. & Stauffacher, C. V. (1997). A mechanism for toxin insertion into membranes is suggested by the crystal structure of the channel-forming domain of colicin E1. *Structure (London)*, **5**, 443–458.
 27. Lamb, D. C., Nienhaus, K., Arcovito, A., Draghi, F., Miele, A. E., Brunori, M. & Nienhaus, G. U. (2002). Structural dynamics of myoglobin. Ligand migration among protein cavities studied by Fourier transform infrared/temperature derivative spectroscopy. *J. Biol. Chem.* **277**, 11636–11644.
 28. Hubbard, S. J. & Argos, P. (1996). A functional role for protein cavities in domain:domain motions. *J. Mol. Biol.* **261**, 289–300.
 29. Yang, L., Weiss, T. M., Lehrer, R. I. & Huang, H. W. (2000). Crystallization of antimicrobial pores in membranes: magainin and protegrin. *Biophys. J.* **79**, 2002–2009.
 30. Unger, T., Oren, Z. & Shai, Y. (2001). The effect of cyclization of magainin 2 and melittin analogues on structure, function, and model membrane interactions: implication to their mode of action. *Biochemistry*, **40**, 6388–6397.
 31. Matsuzaki, K. (1999). Why and how are peptide-lipid interactions utilized for self-defense? Magainins and tachyplesins as archetypes. *Biochim. Biophys. Acta*, **1462**, 1–10.
 32. Minton, A. P. (1999). Adsorption of globular proteins on locally planar surfaces: II. Models for the effect of multiple adsorbate conformations on adsorption equilibria and kinetics. *Biophys. J.* **76**, 176–187.
 33. Peña, S. V., Hanson, D. A., Carr, B. A., Goralski, T. J. & Krensky, A. (1997). Processing, subcellular localization, and function of 519 (granulysin), a human late T cell activation molecule with homology to small, lytic granule proteins. *J. Immunol.* **158**, 2680–2688.
 34. Rubinson, K. A., Ladner, J. E., Tordova, M. & Gilliland, G. L. (2000). Cryosalts: suppression of ice formation in macromolecular crystallography. *Acta Crystallog. sect. D*, **56**, 996–1001.
 35. Yeates, T. O. (1997). Detecting and overcoming crystal twinning. *Methods Enzymol.* **276**, 344–358.
 36. Van Duyne, G. D., Standaert, R. F., Karplus, P. A., Schreiber, S. L. & Clardy, J. (1993). Atomic structures of the human immunophilin FKBP-12 complexes with FK506 and rapamycin. *J. Mol. Biol.* **229**, 105–124.
 37. Hendrickson, W. A. (1999). Maturation of MAD phasing for the determination of macromolecular structures. *J. Synchrotron Radiat.* **6**, 845–851.
 38. Otwinowski, Z. & Minor, W. (1997). Processing of diffraction data collected in oscillation mode. *Methods Enzymol.* **276**, 307–326.
 39. Usón, I. & Sheldrick, G. M. (1999). Advances in direct methods for protein crystallography. *Curr. Opin. Struct. Biol.* **9**, 643–648.
 40. Otwinowski, Z. (1991). Maximum likelihood refinement of heavy atom parameters. In *Daresbury Study Weekend Proceedings*, pp. 80–86, Daresbury Laboratory, Warrington, UK.
 41. Collaborative Computing Project number 4 (1994). The CCP4 suite: programs for protein crystallography. *Acta Crystallog. sect. D*, **50**, 760–763.
 42. Cowtan, K. (1994). 'dm': An automated procedure for phase improvement by density modification. *Joint CCP4 ESF-EACBM Newsletter Protein Crystallog.* **31**, 34–38.
 43. Lamzin, V. S. & Wilson, K. S. (1997). Automated refinement for protein crystallography. *Methods Enzymol.* **277**, 269–305.
 44. Sheldrick, G. M. & Schneider, T. R. (1997). SHELXL: high resolution refinement. *Methods Enzymol.* **277**, 319–343.
 45. Allen, F. H., Davies, J. E., Galloy, J. J., Johnson, O., Kennard, O., Macrae, C. F. *et al.* (1991). The development of versions 3 and 4 of the Cambridge Structural Database System. *J. Chem. Inf. Comput. Sci.* **31**, 187–204.
 46. Kleywegt, G. & Jones, T. A. (1998). Databases in protein crystallography (CCP4 Proceedings). *Acta Crystallog. sect. D*, **54**, 1119–1131.
 47. Laskowski, R. A., MacArthur, M. W., Moss, D. S. & Thornton, J. M. (1993). PROCHECK: a program to check the stereochemical quality of protein structures. *J. Appl. Crystallog.* **26**, 283–291.
 48. Hooft, R. W. W., Vriend, G., Sander, C. & Abola, E. E. (1996). Errors in protein structures. *Nature*, **381**, 272.
 49. Ramachandran, G. N., Ramakrishnan, C. & Sasisekharan, V. (1963). Stereochemistry of polypeptide chain conformations. *J. Mol. Biol.* **7**, 95–99.
 50. Kleywegt, G. J. & Jones, T. A. (1994). Detection, delimitation, measurement and display of cavities in macromolecular structures. *Acta Crystallog. sect. D*, **50**, 178–185.
 51. Guex, N. & Peitsch, M. C. (1997). SWISS-MODEL and the Swiss-PdbViewer: an environment for comparative protein modeling. *Electrophoresis*, **18**, 2714–2723.
 52. Peitsch, M. C. (1996). ProMod and Swiss-Model: internet-based tools for automated comparative protein modelling. *Biochem. Soc. Trans.* **24**, 274–279.
 53. Berman, H. M., Westbrook, J., Feng, Z., Gilliland, G., Bhat, T. N., Weissig, H. *et al.* (2000). The Protein Data Bank. *Nucl. Acids Res.* **28**, 235–242.
 54. Kraulis, P. J. (1991). Molscript: a program to produce both detailed and schematic plots of protein structures. *J. Appl. Crystallog.* **24**, 946–950.
 55. McRee, D. (1999). *Practical Protein Crystallography*, 2nd edit., Academic Press, San Diego.
 56. Merritt, E. A. & Bacon, D. J. (1997). Raster3D: photo-realistic molecular graphics. *Methods Enzymol.* **277**, 505–524.

Edited by D. Rees

(Received 20 June 2002; received in revised form 22 October 2002; accepted 27 October 2002)